Entropy-driven order in an array of nanomagnets

Hilal Saglam[1], Ayhan Duzgun[2], Aikaterini Kargioti[1], Nikhil Harle[3], Xiaoyu Zhang[1], Nicholas S. Bingham[1], Yuyang Lao[4], Ian Gilbert[4,5], Joseph Sklenar[4,6], Justin D. Watts,[7,8] Justin Ramberger[7], Daniel Bromley[9], Rajesh V. Chopdekar[10], Liam O'Brien[9], Chris Leighton[7], Cristiano Nisoli[**,2], and Peter Schiffer[**,1,3,4]

[1]Department of Applied Physics, Yale University, New Haven, CT 06511, USA

[2]Theoretical Division and Center for Nonlinear Studies, Los Alamos National Laboratory, Los Alamos, NM 87545, USA

[3]Department of Physics, Yale University, New Haven, CT 06511, USA

[4]Department of Physics, University of Illinois at Urbana-Champaign, Urbana, IL 61801, USA

[5]Seagate Research Group, Seagate Technology, Shakopee, MN 55379, USA

[6]Department of Physics and Astronomy, Wayne State University, Detroit, MI 48201, USA

[7]Department of Chemical Engineering and Materials Science, University of Minnesota, Minneapolis, Minnesota 55455, USA

[8]School of Physics and Astronomy, University of Minnesota, Minneapolis, Minnesota 55455, USA

[9]Department of Physics, University of Liverpool, Liverpool L69 3BX, United Kingdom

[10]Advanced Light Source, Lawrence Berkeley National Laboratory, Berkeley, CA 94720, USA

[**]Corresponding authors: peter.schiffer@yale.edu and cristiano@lanl.gov

Long-range ordering is typically associated with a decrease in entropy. Yet, it can also be driven by increasing entropy in certain special cases. We demonstrate that artificial spin ice arrays of single-domain nanomagnets can be designed to produce entropy-driven order. We focus on the tetris artificial spin ice structure, a highly frustrated array geometry with a zero-point Pauli entropy, which is formed by selectively creating regular vacancies on the canonical square ice lattice. We probe thermally active tetris artificial spin ice both experimentally and through simulations, measuring the magnetic moments of the individual nanomagnets. We find two-dimensional magnetic ordering in one subset of these moments, which we demonstrate to be induced by disorder (i.e., increased entropy) in another subset of the moments. In contrast with other entropy-driven systems, the discrete degrees of freedom in tetris artificial spin ice are binary and are both designable and directly observable at the microscale, and the entropy of the system is precisely calculable in simulations. This example, in which the system's interactions and ground state entropy are well-defined, expands the experimental landscape for the study of entropy-driven ordering.

The somewhat paradoxical phenomenon of long-range ordering driven by maximizing entropy is observed in only a few systems in nature [1], such as vibrofluidized hard spheres, in which ordering maximizes the spheres' so-called free volume [2,3]. Often, ordering in one subset of degrees of freedom is driven by the possibility of increasing entropy in another subset, and thus of the total entropy. For instance, in the thin rod model of Onsager [4], rods order nematically to increase their translational entropy [5,6,7,8]. Entropy-driven ordering has been demonstrated primarily in out-of-equilibrium soft matter systems such as colloids, hard sphere suspensions, and liquid crystals, where it has importance in self-assembly [9,10] for systems of biological and technological relevance [3,5,8,11,12,13,14]. Furthermore, entropy maximization is also implicated in the formation of high entropy alloys of metallurgical importance [15].

While these effects have been studied in chemistry and in the physics of soft matter, a related yet different phenomenon in magnetic materials, so-called "order-by-disorder" [16,17], pertains instead to the interaction of spins arranged on a lattice in magnetic materials where collective excitations among magnetic moments select an ordered, rather than disordered, configuration in the ground state [18,19,20,21,22,23].

Here we report entropy-driven ordering in an artificial spin ice, a structurally ordered nanomagnet array [24,25]. Specifically, we examine entropy-driven ordering in tetris artificial spin ice (referred to as 'tetris ice' for the remainder of the paper) [26,27]. We demonstrate a different paradigm for such ordering, quite distinct from what has been previously observed. Crucially, ordering in this system has strong similarities to the soft

matter systems described above, despite tetris ice being a structured nanomagnet array with no mechanical motion. Its degrees of freedom are, instead, the binary orientations of the nanoscale moments that are configured through thermalization.

Artificial spin ices can serve as models for a wide range of unusual physics unavailable in other systems, because they are lithographically designed at will. The ability to probe the magnetic degrees of freedom at the resolution of a single magnetic moment has provided the first realizations of celebrated vertex models [28] and also led to experimental demonstrations of a number of new models for collective behavior [24,25,29]. Relevant to our study, the characteristic that the individual magnetic degrees of freedom are constrained to point in one of two directions for each moment, sets tetris ice apart from the entropy-driven orderings referenced above.

The structure of tetris ice is obtained by selective removal of moments from the canonical square ice structure, as illustrated in Figure 1a and 1b. This system belongs to a category of artificial spin ices that are ‘vertex-frustrated’ [26,29], i.e., they are structured such that every lattice vertex cannot have its moments arranged in their local low energy configuration. As a result, the system necessarily has multiple ‘unhappy vertices’ that are excited out of their local vertex ground states, as well as zero-point entropy associated with the degeneracy in allocating the unhappy vertices within the lattice.

We start our discussion of the collective states of tetris ice with a description of the energy and entropy of moment configurations at low energy. As indicated in Figure 1b, the

system's lowest energy manifold is composed of two different one-dimensional subsystems of alternating stripes of moments, so-called 'backbones' and 'staircases' [26,27]. In the system's ground state, the staircase (*SC*) moments contain unhappy vertices and are disordered. Moreover, the individual staircase zero-temperature disorder, and thus its correlations, are well-described by a disordered one-dimensional Ising phase [27]. In contrast, the backbone (*BB*) moments do not contain any unhappy vertices, and are ordered longitudinally, i.e., along the length of the stripes. Within a nearest neighbor coupling approximation, a given ground state configuration of the array receives no energetic advantage from being *transversely* ordered, meaning that mutual order among the different backbones is neither energetically favored nor disfavored [26].

In order to characterize ordering among the backbone moments, we use the staggered order parameter, $\Psi = (-1)^{i+j} S_{ij}^{BB}$, where S_{ij}^{BB} denotes the polarization of the backbone moments, and *i* and *j* are the vertical and horizontal location indices of the moments in the underlying square ice lattice [28]. Note that Ψ here is simply the standard antiferromagnetic order parameter for the ordering of square ice: the average value $\langle\Psi\rangle = \pm 1$ corresponds to the two equivalent ordered ground states of that lattice. In other words, two ordered backbones have the same $\langle\Psi\rangle$ if their moments' orientations belong to the same ground state of the underlying square lattice.

In Figure 2a, we schematically illustrate the case of neighboring backbones in the ground state with the same $\langle\Psi\rangle$. It has been proven that, in this configuration, the ground state of the staircase moments between the backbones is necessarily disordered [26]. An

alternative ground state for the system has neighboring backbones alternating their values of $\langle\Psi\rangle$ between ±1, as shown in Figure 2b. In this other ground state configuration, the staircase moments between the backbones must be ordered [26]. These two alternative ground state configurations have the same energy, but the disorder in the staircases of the former gives an entropic advantage for neighboring backbones to have the same value of $\langle\Psi\rangle$. Thus, there is an entropic advantage for the entire two-dimensional system to have all backbones with either $\langle\Psi\rangle = 1$ or $\langle\Psi\rangle = -1$, implying two-dimensional order among the backbone moments. In other words, the backbones order to the same $\langle\Psi\rangle$ to gain global entropy for the system, which comes from the entropy of the disordered staircase moments. The system sacrifices the entropy that it would gain by having randomness in the value of $\langle\Psi\rangle$ among different backbones, because that entropy scales subextensively (since $\langle\Psi\rangle$ is binary, the entropy of a backbone-disordered configuration is proportional to the number of backbones in the system, which scales as the square root of the area of the array). In doing so, the system gains entropy from the staircases, which instead scales extensively, i.e., with the system size, as shown in the Supplementary Information (Section 5).

Entropy maximization implies mutual transverse ordering among backbones, but it also explains the longitudinal ordering within a single backbone. Consider a configuration of ordered backbones all with the same $\langle\Psi\rangle$, in which one backbone has a finite longitudinal domain of length L_d with opposite $\langle\Psi\rangle$, as in Figure 2c. The two defects induce two ordered regions on the adjacent staircases, above and below the domain, corresponding to an approximate increase in the staircase free energy $\Delta F = K + TL_d s_{sc}$, where K is the energy

of the domain boundaries, T is the system temperature, and s_{sc} is the entropy per moment of the disordered staircase (see Supplementary Materials Section 5). This entropic term in the free energy yields a constant attraction $\sim T s_{sc}$ among the two defects, suppressing the growth of the bound domain. This purely entropic interaction is crucial to explain the individual longitudinal ordering of the backbones since, as a one-dimensional system, a single backbone would not be expected to order without this attractive interaction among defects. Using similar reasoning, one can show that defects on neighboring backbones also interact entropically, favoring their alignment into two-dimensional domain walls (Figure 2d).

We now turn to experimental studies of this system. We have experimentally investigated the entropy-driven ordering in tetris ice through X-ray magnetic circular dichroism photoemission electron microscopy (XMCD-PEEM) measurements on three samples of tetris ice composed of thin permalloy ($Ni_{80}Fe_{20}$) nanoislands. The thickness (~3 nm) was chosen so that the island moments were thermally active in the measurement temperature range, i.e., thermal moment reversals occurred on the time scale of imaging. The samples (A, B, and C) had different interaction strengths between neighboring moments, associated with differences in the island size and spacing. Sample A (studied previously [27]) had the strongest interactions and sample C had the weakest interactions, based on micromagnetic calculations [30]. A representative scanning electron microscope image is shown in Figure 1a, and detailed descriptions of the samples and measurements are given in the Methods Section and the Supplementary Information (Section 1).

The XMCD-PEEM technique allows full-field imaging of moment orientations in the lattice on time scales of the order of seconds. A typical XMCD-PEEM image is shown in Figure 1c and the corresponding map of moment directions in Figure 1d. In the temperature range studied for each sample (see Section 2 in the Supplementary Information for details), the system ranged from having the moments fluctuating faster than the images could capture at the highest temperatures, to the moments being effectively frozen at the lowest temperatures. We note that this technique has been demonstrated previously to effectively thermalize the moments in artificial spin ice [31] and has been used extensively under the assumption of thermalization [24,25]. For all of the samples, the temperature dependence of the average vertex statistics is quite small, suggesting that the system thermalized at room temperature, and relaxed upon cooling to a metastable moment configuration within which the moments fluctuated without further reducing the overall system energy. This suggests that further relaxation to the ground state is limited by the complex topology of the lattice [32,33], in combination with intrinsic structural disorder associated with limitations of the lithography.

In Figures 3a and 3b, we show a schematic of the digitized moment configurations obtained from XMCD-PEEM measurements of two samples with different interaction strengths and therefore different proximity to the ground state. Figure 3a shows a moment configuration close to the ground state, demonstrating close to full two-dimensional ordering of the backbones, coexisting with disorder in the staircases. Note that the ordered configurations in the backbones correspond to those of the antiferromagnetic ground state of square ice from which the tetris ice structure is

obtained, but the disordered moments on the staircases do not. This ordering is apparent in the series of so-called “type-I” vertices [2] along the backbones that correlate both along the backbones and across them, leading to visible structure in the moment orientation, i.e., the formation of near-complete loops of approximate head-to-tail flux-closure in the moment orientations, broken only by disorder on the staircases. Such structure can also be seen to a lesser extent in Figure 3b, which shows a moment configuration somewhat further from the ground state with domain walls in the backbones between regions of different $\langle\Psi\rangle$.

In Figure 3c, we show the resulting order parameter $\langle\Psi\rangle$ as a function of the average vertex energy for the different samples, noting that the different interaction strengths associated with the differences among the samples lead to different energies in the thermalized states. The average vertex energy, E_{avg}, is defined as $E_{avg} = \sum \varepsilon_\alpha N_\alpha / N_{total}$, where N_α is the number of observed vertices of type α, ε_α is the vertex energy, and N_{total} is the total number of vertices. The vertex energies, ε_α, were calculated using micromagnetic simulations [30] for different vertices, lattice constants, and island dimensions (see Section 3 in the Supplementary Information for details). The numbers of vertices, N_α, were extracted from the XMCD-PEEM data. Since the temperature dependence of the vertex statistics was weak, we show data averaged over the full temperature range in which we took data (see Section 2 in the Supplementary Information for details).

Because $\langle\Psi\rangle$ in Figure 3c is measured over the entire image, its increasing value with stronger interaction energy corresponds to a transverse ordering of the moments in the backbones. In Figure 3d, we plot the fractional flipping rate of different moments in the system as a function of the interaction energy (defined as the fraction of the moment flips between successive frames that are among the backbone moments, vertical staircase moments, and horizontal staircase moments, respectively). The results show that kinetics are largely confined to the disordered staircases, especially for the largest magnitude interaction energies.

We now analyze the longitudinal and transverse correlations to quantify the two-dimensional order across the system. If S_{ij}^{BB} and $S_{i'j'}^{BB}$ are two backbone moments, we define their transverse and longitudinal correlations as $C_{BB} = S_{ij}^{BB} S_{i'j'}^{BB} (-1)^{i-i'+j-j'}$, where C_{BB} = +1 if the moments have the same value of Ψ and C_{BB} = -1 if the values of Ψ are opposite. For both horizontal and vertical staircase moments, we instead define the usual ferromagnetic correlation, i.e., $C_{SC} = S_{ij}^{SC} S_{i'j'}^{SC}$. Since we are primarily interested in longer-range correlations, we consider only those horizontal staircase moments where the two adjacent moments in a step are aligned head to tail.

In Figure 4, we show measured correlations among different moment pairs for the three samples, again averaged over all temperatures; the error bars here represent standard deviations of the data collected at different temperatures. Figure 4a defines the pairs of nearest and next-nearest neighbor moments, both longitudinally and transversely, through color labels (similar definitions are in Figures 4d and 4g). Figure 4b plots

longitudinal correlations of horizontal moments within the same staircases. Note that the distance dependence of the longitudinal moment correlations within the horizontal staircases does not change much among the samples, because those correlations are a property of the constrained disorder of the ground state. By contrast, there are considerable differences among the three samples in the longitudinal correlations within the backbones (Figure 4e). They become increasingly more correlated with increasing interaction strength (from C to B to A), and the correlations evolve to an almost flat $\langle C_{BB} \rangle$ = 1 value as a function of distance for sample A, as expected for the ground state.

We now consider correlations transverse to the backbones and staircases. Figure 4c shows no discernable transverse correlation among the horizontal moments of different staircases. In contrast, Figure 4f reveals considerable transverse correlations among backbone moments, with correlation values almost as large as the longitudinal case (Figure 4e). As in that case, they grow with increasing interaction strength, eventually approximating the flat $\langle C_{BB} \rangle$ = 1 value that corresponds to two-dimensional long-range order. This can be seen clearly in real space snapshots that reveal isotropic domains of various sizes (see Figure SI. 2.6 – 2.8). The contrasting complete lack of transverse order among the horizontal staircase moments is a clear indication of the separation of the backbones and the staircases in terms of their entropy – with the entropy of the backbones minimized and the entropy of the staircases (and thus of the whole system) maximized. Note that, because the staircases separate the backbones, the impressive ordering of the backbone moments is strong evidence for the entropically-mediated interactions among the backbones. Our Monte Carlo simulations, discussed below, show

that a near-neighbor model, with no interaction whatsoever among backbones, replicates these experimental findings (See Figure SI. 4.2).

Completing our discussion of Figure 4, the correlations among the vertical moments in the staircases are shown in Figures 4h and 4i. We observe that the correlation among the vertical moments is almost flat in magnitude (but alternating in sign), as if they were ordered, but the value of the correlation is $|\langle C_{SC}\rangle|$ ~ 0.5 for sample A, and smaller for samples B and C. These moments thus possess features of both long-range order (correlation almost constant in space) as well as disorder, in the sense that $|\langle C_{SC}\rangle|$ never approaches unity, even for near neighbors. As shown in the Supplementary Information (see Section 6), correlations among vertical staircase moments are dictated by both horizontal staircase moments, which are disordered, and also by the backbone moments surrounding the staircases, which are ordered; a value of $|\langle C_{SC}\rangle| = 0.5$ is expected in the system ground state. This sort of *half-ordering* of the vertical moments is highly unusual in magnetic systems: it is neither short-range ordering, which should approach $|\langle C_{SC}\rangle|$ ~ 1 at short distances along a given lattice direction and fall sharply with increasing separation, nor a disordered state, as the absolute value of the correlation persists at nearly the same value with distance. Rather, this represents a consequence of the peculiar frustration in tetris ice.

We now discuss simulations of this system, which enhance our understanding of the experimental results. The attribution of transverse ordering to entropic effects assumes that the ordering is not arising from long-range interactions among the moments. To

confirm that long-range interactions are not needed to explain the ordering, we have performed Metropolis Monte Carlo simulations within a vertex model that considers only interactions among moments that share a common vertex. This excludes interactions among the moments belonging to different backbones and staircases, and thus provides an important corroboration of the entropy-induced mechanism of the backbone ordering. Significantly, because the Monte Carlo produces a collective state that mirrors what we see in experiment, it provides a separate validation that our experimental system was well thermalized (details of the Monte Carlo results are given in the Supplementary Information, Section 4).

Figure 5a shows the entropy, the specific heat and the order parameter $\langle \Psi \rangle$ from our simulations, as a function of temperature. We note the sharp peak in the specific heat, associated with ordering of the backbones (a transition that is inaccessible in our XMCD-PEEM temperature range). The transition temperature corresponds to the energy scale of vertex interaction energies, which indicates that longer-range interactions are not driving the transition, a conclusion that is also suggested by the disorder on the staircase moments. The observation of both an ordering transition among the backbone moments, a disordered state among the staircase moments, and a residual entropy for the system, which must be associated with that disorder, shows the clear separation of the entropy among the two subsets of moments. Because the backbone moments are ordered, this simulation also provides a quantification of the entropy associated with the staircase disorder.

Figure 5b plots the corresponding temperature dependence of the moment fractional flip rates, showing how the dynamics of the system below the ordering temperature are confined to the staircase moments. Note that the fractional flip rates for both vertical and horizontal staircases are non-zero at the lowest temperatures and the vertical staircase fractional flip rate rises continuously as the temperature decreases, suggesting that those are the most active moments. This again points to the distinct behavior of the backbone and staircase moments within the tetris ice structure, despite being strongly correlated.

We also use our Monte Carlo simulations to demonstrate entropy-based ordering in a situation that cannot be easily reproduced experimentally. Specifically, we initiate the system in a ground state configuration corresponding to an order parameter of zero, i.e., $\langle\Psi\rangle = \pm 1$ on alternating backbones (see Figure SI. 4.3a). We then allow the system to evolve at a temperature of only ~0.3 T_C, where T_C is the ordering temperature for the backbones. Our simulations show that the system spontaneously evolves through thermal fluctuations into a backbone-ordered state corresponding to uniform $\langle\Psi\rangle = 1$ (see Figure SI. 4.3b). This further supports the robust nature of the observed entropically-driven ordering among backbone moments since it can be obtained through multiple thermodynamic paths, not just through cooling from high temperature.

We now compare our entropy-driven ordering with similar phenomena in other systems. Our observed ordering in the tetris ice system is substantially different from the so-called ‘order-by-disorder’ in some other magnetic systems [16-23]. In those cases, fluctuations can lift the degeneracy of the ground state by selecting ordered states of lower energy

excitation. In our case, however, the very ground state manifold at zero temperature ‘favors’ order, because this order maximizes the residual entropy that results from frustration. Indeed, configurations with ordered backbones numerically dominate the ground state manifold in the large size limit, as we demonstrate in the Supplementary Information (see Section 5).

The tetris ice system is therefore conceptually closer in nature to the entropy-based ordering seen in the structurally-disordered materials, where some degrees of freedom become ordered to enable more entropy in other degrees of freedom. A paradigmatic example is the nematic ordering of rod-shaped objects in the seminal Onsager model [1,4]. The tetris ice system similarly has two distinct and competing entropies, that of the staircase moments and that of the backbone moments. The latter is reduced to maximize the former, a mechanism which maximizes the *total* entropy, analogous to the Onsager model. An important difference, however, is that the tetris ice system is well structured around a specific geometry, with discrete degrees of freedom that are experimentally accessible. While the two entropies correspond in the Onsager model to different coordinates of the same rods, in tetris ice they refer to different positions in a lattice. The two cases are mathematically similar in that the entropy of a subset of degrees of freedom is reduced to maximize the total entropy, but the nature of the degrees of freedom are strikingly different, mechanical and continuous in the former, binary in the latter, distinctly separating the two cases.

Many groups have now established that frustration in a magnetic system can result in a residual entropy, with the spin ice pyrochlore materials providing an excellent example [34]. Our findings go considerably further, demonstrating that such residual entropy can drive robust ordering in a frustrated magnetic system. This suggests that a range of other artificial spin ice geometries could be designed to tune the balance between energetic and entropic effects in ordering of moments, a possibility that would be quite difficult to realize in other physical systems.

The observation of entropy-driven magnetic ordering in the tetris ice system also adds a new category to the types of systems that display entropy-driven ordering. While our experiments are driven purely through thermal effects, the addition of quantum fluctuations [35] will likely drive yet more exotic phenomena associated with entropic considerations. Future studies will be able to probe additional bespoke artificial spin ice structures with ground state entropy that favors other types of ordering phenomena. More generally, our results show how non-trivial forms of frustration can be used to generate unusual, even apparently paradoxical phenomena that are broadly related to other physical phenomena in disparate systems [1], and to do so in ways that enable more detailed studies of the microscopic driving behavior.

ACKNOWLEDGEMENTS

We thank I.-A. Chioar for fruitful discussions and A. Scholl for assistance with the early XMCD-PEEM measurements. Work at Yale University and the University of Illinois at Urbana-Champaign was funded by the US Department of Energy (DOE), Office of Basic Energy Sciences, Materials Sciences and Engineering Division under Grant No. DE-SC0010778 and Grant No. DE-SC0020162 [H.S., A.K., N.H., X.Z., N.S.B., Y.L., I.G., J. S., and P.S.]. This research used resources of the Advanced Light Source, a DOE Office of Science User Facility under contract no. DE-AC02-05CH11231 [R.C.]. Work at the University of Minnesota was supported by NSF through Grant Nos. DMR-1807124 and DMR-2103711 [J.R., J.D.W., and C. L.]. Work at the University of Liverpool was supported by the UK Royal Society, Grant No. RGS\R2\180208 [D.B. and L. O.]. Work at Los Alamos National Laboratory was carried out under the auspices of the US DOE through LANL, operated by Triad National Security, LLC (Contract No. 892333218NCA000001) and financed by DOE LDRD [A.D. and C.N.].

AUTHORS' CONTRIBUTIONS

J. Ramberger and J. D. Watts performed film depositions under the guidance of C. Leighton, and D. Bromley prepared other samples under the guidance of L. O'Brien, with H. Saglam, X. Zhang, I. Gilbert, Y. Lao, J. Sklenar, and N. S. Bingham overseeing the lithography. H. Saglam, X. Zhang, I. Gilbert, Y. Lao, J. Sklenar, N. S. Bingham and R.V. Chopdekar performed the XMCD-PEEM characterization of the thermally active samples, and H. Saglam, A. Kargioti, and N. Harle analyzed the data. H. Saglam performed micromagnetic calculations. A. Duzgun performed Monte Carlo simulations, under the guidance of C. Nisoli. C. Nisoli and P. Schiffer supervised the entire project. All authors contributed to the discussion of results and to the finalization of the manuscript.

COMPETING INTERESTS

The authors declare no competing interests.

DATA AVAILABILITY

Underlying data are available at the following URL: https://datadryad.org/stash/share/-sT0veB190OcBSNk3G_ZW1qMa1yjbu7zjZhs-galmV0.

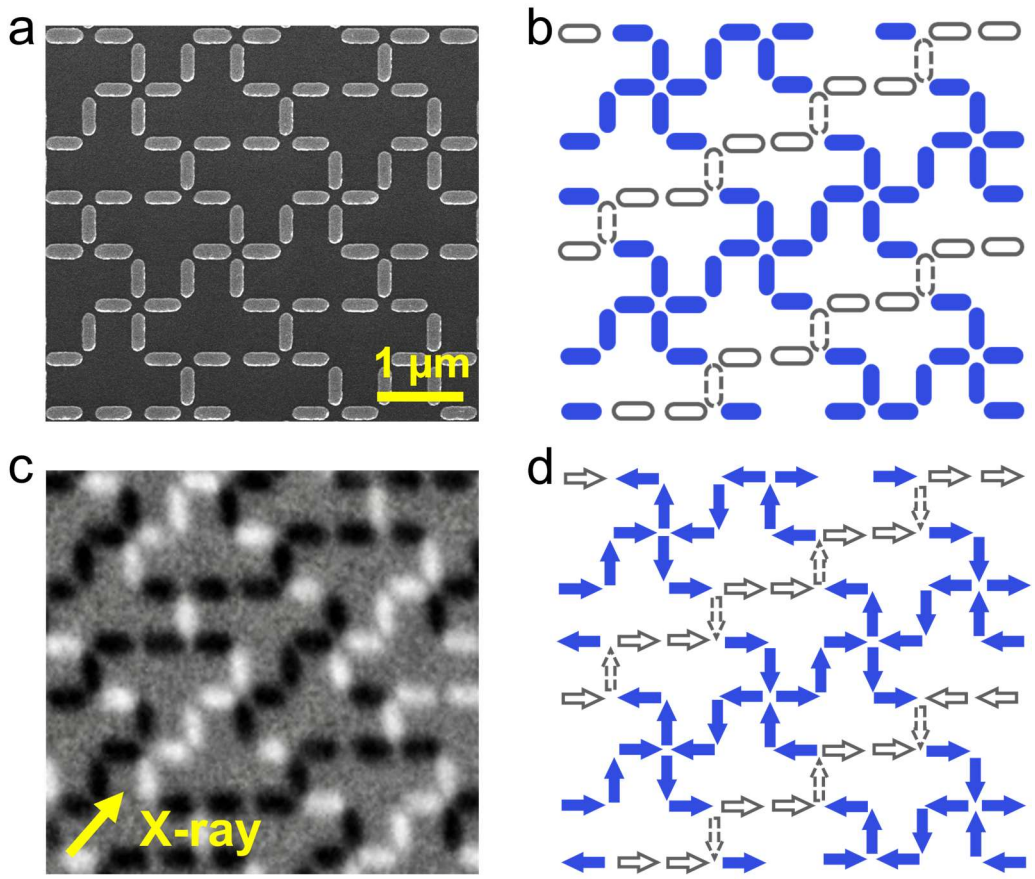

Figure 1: Tetris Artificial Spin Ice. **(a)** Scanning electron microscope (SEM) image of a tetris artificial spin ice (sample A). **(b)** Schematic of the tetris ice structure in which backbone nanomagnet islands are in blue and staircase islands are in grey, with the vertical moments having dashed borders and the horizontal moments having solid borders. The *longitudinal direction* is defined as the direction parallel to the stripes, approximately 26.5° degrees from the horizontal, and the *transverse direction* perpendicular to that. **(c)** X-ray magnetic circular dichroism-photoemission electron microscopy (XMCD-PEEM) image of the tetris ice lattice, where the direction of the incident X-ray beam is indicated by the yellow arrow. The islands that have a magnetization component along (opposite) the X-ray direction yield black (white) contrast (sample A at T = 120 K). **(d)** Map of magnetic moment configuration corresponding to the XMCD-PEEM image in (c) with the same color scheme as (b).

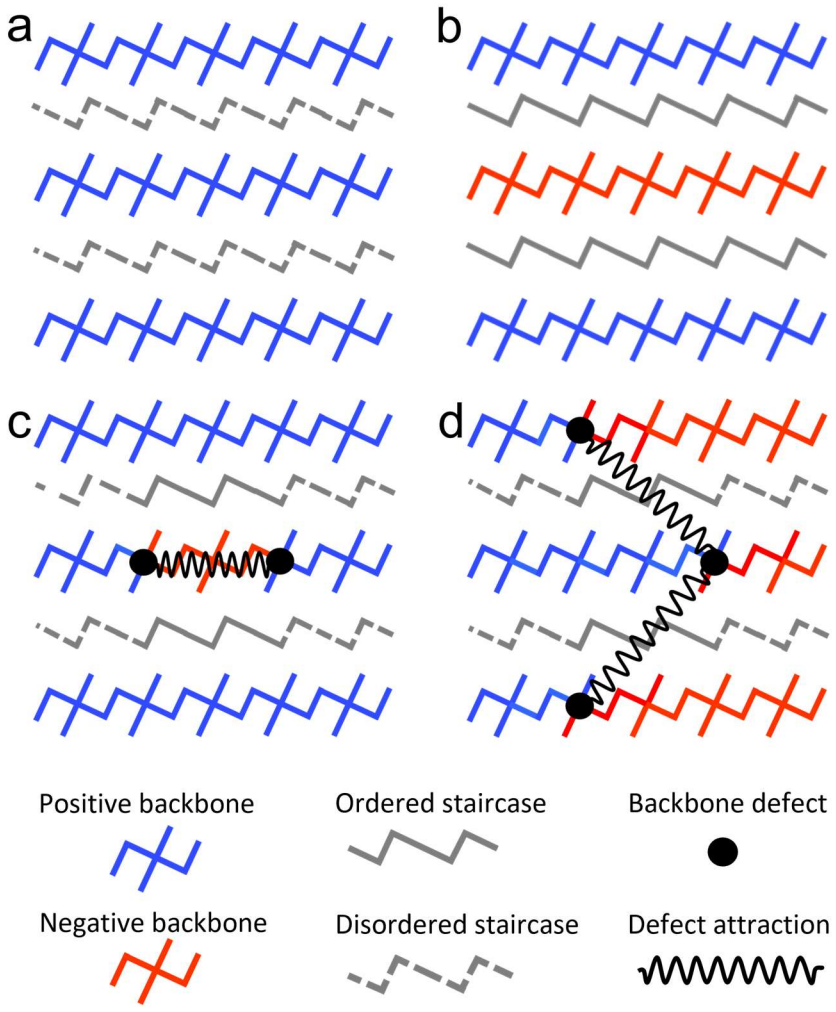

Figure 2: Entropic Interactions in Tetris Ice. **(a)** Schematic of a ground state configuration that leads to maximal disorder in staircases due to the transverse ordering among the backbones, all having the same $\langle\Psi\rangle$. **(b)** Schematic of a ground state configuration where backbones alternate their order parameter $\langle\Psi\rangle$, leading to the staircase moments being ordered. **(c)** Schematic of backbone defect attraction where two longitudinal defects attract each other due to the entropy cost of ordering portions of the adjacent staircases. **(d)** Schematic of backbone defect attraction across multiple backbones, where backbone defects attract each other due to the entropy cost of ordering portions of the adjacent staircases, thus favoring two-dimensional domain walls that cross multiple backbones. Moment orientations that correspond to these schematics are given in the Supplementary Information (Figure SI. 2.5)

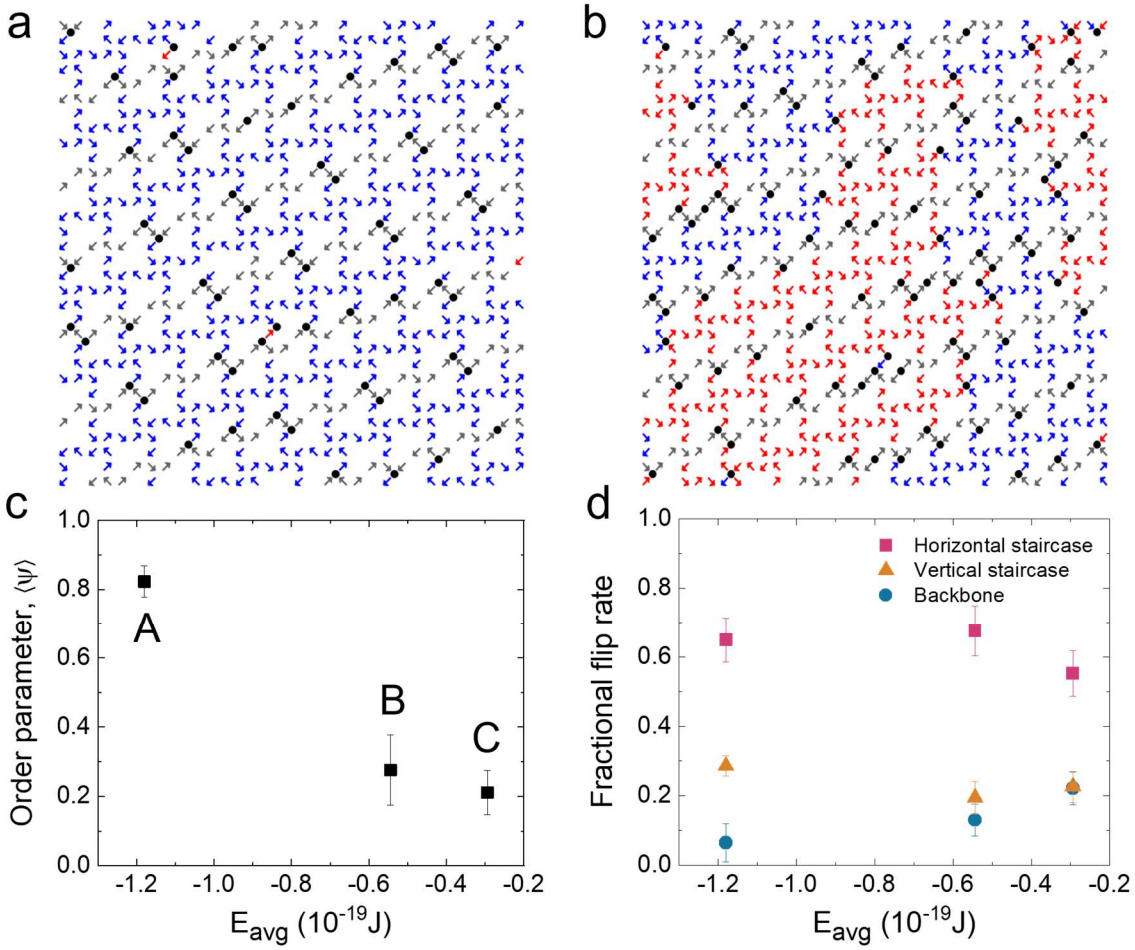

Figure 3: Two-dimensional Ordering in Tetris Ice. **(a)** Digitized XMCD-PEEM snapshot of tetris ice near the ground state, showing single-domain ordering of the backbones (sample A at T = 120 K). **(b)** Digitized XMCD-PEEM snapshot of tetris ice above the ground state, showing backbones ordering in two-dimensional domains, while the staircases remain disordered (sample B at T = 190 K). The black dots indicate unhappy vertices. **(c)** Staggered antiferromagnetic order parameter for the backbone moments plotted as a function of increasing average vertex energy from Sample A to C. **(d)** Relative probability of flipping for backbone, horizontal and vertical staircase islands, i.e., the fractional flip rate, showing that more than 80% of the kinetics is in the staircases. The error bars represent standard deviations of the data collected at different temperatures.

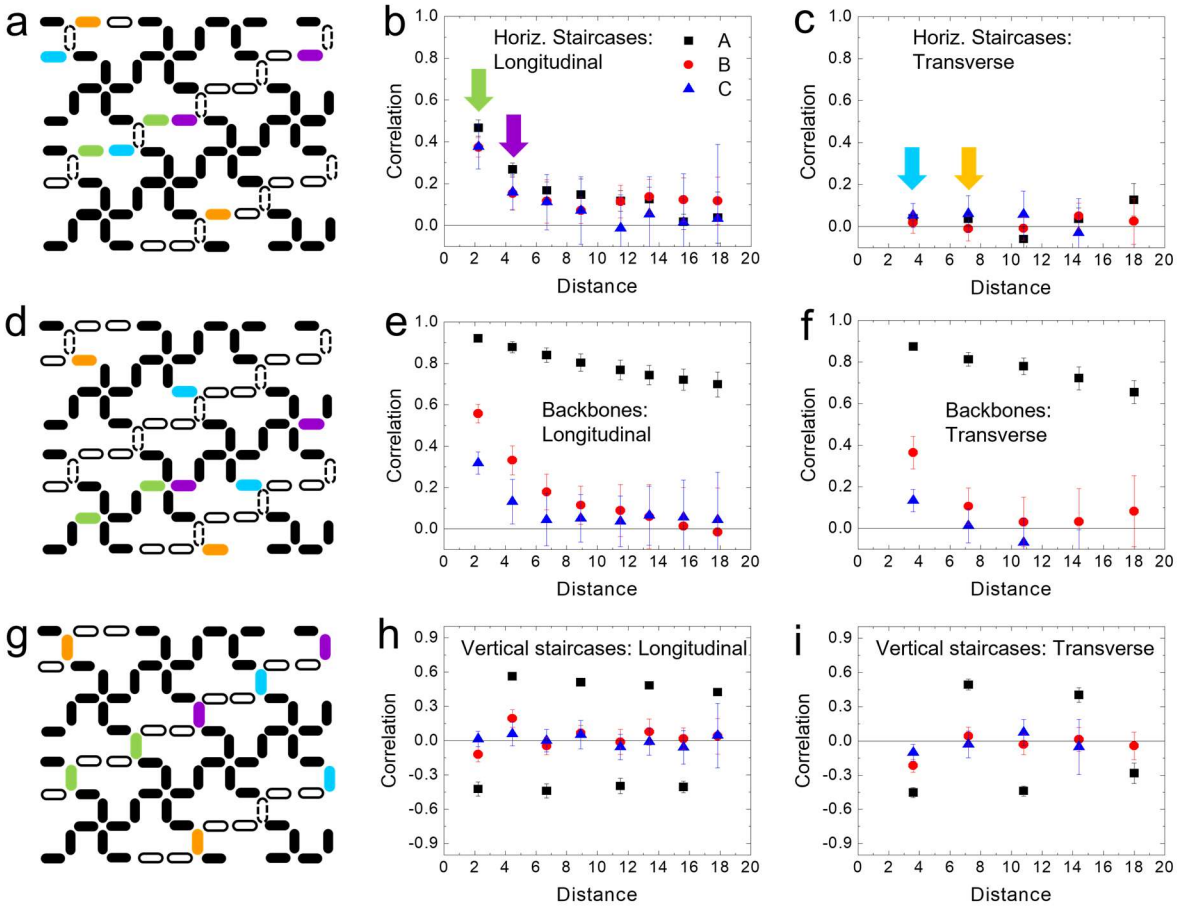

Figure 4: Longitudinal and Transverse Moment Correlations. (a) Schematic of the tetris ice structure highlighting the horizontal staircase islands. The two horizontal staircase islands that are each other's nearest neighbors in the longitudinal direction are colored in green. The two horizontal staircase islands that are each other's nearest neighbor in the transverse direction are colored in blue. Similarly, purple and orange indicate the next-nearest neighbors in the longitudinal and transverse directions, respectively. Note that we do not consider the pairs of horizontal moments that are within a particular stair of the staircases, since such pairs are highly correlated. **(b)** The average moment correlations as a function of distance (in the units of the lattice constant of the underlying square ice lattice structure) within horizontal staircases (longitudinal correlations) for the three samples studied. **(c)** The average moment correlations as a function of distance across the horizontal staircases (transverse correlations) for the three samples studied. **(d,e,f)** The equivalent schematics and plots as in (a,b,c) but for the backbone moments. **(g,h,i)** The equivalent schematics as in (a,b,c) but for the vertical staircase moments. The error bars represent standard deviations of the data collected at different temperatures.

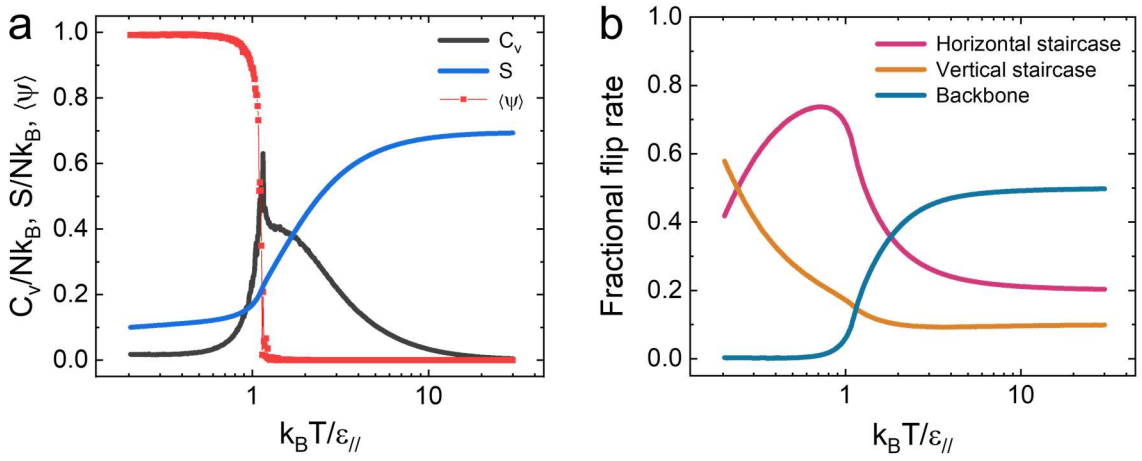

Figure 5: Two-dimensional-Ordering in Tetris Ice - Simulation. **(a)** Specific heat (C_v), entropy (S), and order parameter $\langle\Psi\rangle$ for the backbone moments vs. temperature computed via Monte Carlo simulations (details provided in the Supplementary Information (see Section 4)). The specific heat shows a peak corresponding to the entropy-induced ordering transition of the backbones, while the entropy shows a residual value at zero temperature that is associated with the staircases. **(b)** The temperature dependence of the moment fractional flip rates for different types of moments in the lattice.

REFERENCES

1. D. Frenkel, Order through entropy, Nature Materials **14**, 9 (2015).

2. Percus, J. K. (ed.) The Many-Body Problem (Interscience, 1963).

3. K.-H. Lin, J. C. Crocker, V. Prasad, A. Schofield, D. A. Weitz, T. C. Lubensky, and A. G. Yodh, Entropically driven colloidal crystallization on patterned surfaces, Physical Review Letters **85**, 1770 (2000).

4. L. Onsager, The effects of shape on the interaction of colloidal particles, Annals of the New York Academy of Sciences **51**, 627 (1949).

5. S. Fraden, G. Maret, D. L. D. Caspar, and R. B. Meyer, Isotropic-nematic phase transition and angular correlations in isotropic suspensions of tobacco mosaic virus, Physical Review Letters **63**, 2068 (1989).

6. D. van der Beek and H. N. W. Lekkerkerker, Nematic ordering vs. gelation in suspensions of charged platelets, Europhysics Letters **61**, 702 (2003).

7. S. Dussi and M. Dijkstra, Entropy-driven formation of chiral nematic phases by computer simulations, Nature Communications **7**, 11175 (2016).

8. K. H. Kil, A. Yethiraj, and J. S. Kim, Nematic ordering of hard rods under strong confinement in a dense array of nanoposts, Physical Review E **101**, 032705 (2020).

9. L. Filion, M. Hermes, R. Ni, E. C. M. Vermolen, A. Kuijk, C. G. Christova, J. C. P. Stiefelhagen, T. Vissers, A. van Blaaderen, and M. Dijkstra, Self-assembly of a colloidal interstitial solid with tunable sublattice doping, Physical Review Letters **107**, 168302 (2011).

10. F. Sciortino, Entropy in self-assembly, La Rivista Del Nuovo Cimento **42**, 511 (2019).

11. P. N. Pusey and W. van Megen, Phase behaviour of concentrated suspensions of nearly hard colloidal spheres, Nature **320**, 340 (1986).

12. E. Barry and Z. Dogic, Entropy driven self-assembly of nonamphiphilic colloidal membranes, Proceedings of the National Academy of Sciences **107**, 10348 (2010).

13. P. F. Damasceno, M. Engel, and S. C. Glotzer, Predictive self-assembly of polyhedra into complex structures, Science **337**, 453 (2012).

14. G. Zhu, Z. Huang, Z. Xu, and L.-T. Yan, Tailoring interfacial nanoparticle organization through entropy, Accounts of Chemical Research **51**, 900 (2018).

15. Y. Zhang, T. T. Zuo, Z. Tang, M. C. Gao, K. A. Dahmen, P. K. Liaw, and Z. P. Lu, Microstructures and properties of high-entropy alloys, Progress in Materials Science **61**, 1 (2014).

16. J. Villain, R. Bidaux, J.-P. Carton, and R. Conte, Order as an effect of disorder, Journal de Physique **41**, 1263 (1980).

17. C. L. Henley, Ordering due to disorder in a frustrated vector antiferromagnet, Physical Review Letters **62**, 2056 (1989).

18. M. E. Zhitomirsky, M. V. Gvozdikova, P. C. W. Holdsworth, and R. Moessner, Quantum order by disorder and accidental soft mode in $Er_2Ti_2O_7$, Physical Review Letters **109**, 077204 (2012).

19. X. Plat, Y. Fuji, S. Capponi, and P. Pujol, Selection of factorizable ground state in a frustrated spin tube: Order by disorder and hidden ferromagnetism, Physical Review B **91**, 064411 (2015).

20. P. C. Guruciaga, M. Tarzia, M. V. Ferreyra, L. F. Cugliandolo, S. A. Grigera, and R. A. Borzi, Field-tuned order by disorder in frustrated Ising magnets with antiferromagnetic interactions, Physical Review Letters **117**, 167203 (2016).

21. K. A. Ross, Y. Qiu, J. R. D. Copley, H. A. Dabkowska, and B. D. Gaulin, Order by disorder spin wave gap in the XY pyrochlore magnet $Er_2Ti_2O_7$, Physical Review Letters **112**, 057201 (2014).

22. A. G. Green, G. Conduit, and F. Krüger, Quantum order-by-disorder in strongly correlated metals, Annual Review of Condensed Matter Physics **9**, 59 (2018).

23. R. Okuma, D. Ueta, S. Kuniyoshi, Y. Fujisawa, B. Smith, C. H. Hsu, Y. Inagaki, W. Si, T. Kawae, H. Lin, F. C. Chuang, T. Masuda, R. Kobayashi, and Y. Okada, Fermionic order by disorder in a van der Waals antiferromagnet, Scientific Reports **10**, 15311 (2020).

24. P. Schiffer and C. Nisoli, Artificial spin ice: Paths forward, Applied Physics Letters **118**, 110501 (2021).

25. S. H. Skjærvø, C. H. Marrows, R. L. Stamps, and L. J. Heyderman, Advances in artificial spin ice, Nature Reviews Physics **2**, 13 (2020).

26. M. J. Morrison, T. R. Nelson, and C. Nisoli, Unhappy vertices in artificial spin ice: new degeneracies from vertex frustration, New Journal of Physics **15**, 045009 (2013).

27. I. Gilbert, Y. Lao, I. Carrasquillo, L. O'Brien, J. D. Watts, M. Manno, C. Leighton, A. Scholl, C. Nisoli, and P. Schiffer, Emergent reduced dimensionality by vertex frustration in artificial spin ice, Nature Physics **12**, 162 (2016).

28. R. J. Baxter, Spontaneous staggered polarization of the F-model, Journal of Statistical Physics **9**, 145 (1973).

29. C. Nisoli, V. Kapaklis, and P. Schiffer, Deliberate exotic magnetism via frustration and topology, Nature Physics **13**, 200 (2017).

30. A. Vansteenkiste, J. Leliaert, M. Dvornik, M. Helsen, F. Garcia-Sanchez, and B. V. Waeyenberge, The design and verification of MuMax3, AIP Advances **4**, 107133 (2014).

31. A. Farhan, P. M. Derlet, A. Kleibert, A. Balan, R. V. Chopdekar, M. Wyss, J. Perron, A. Scholl, F. Nolting, and L. J. Heyderman, Direct observation of thermal relaxation in artificial spin ice, Physical Review Letters **111**, 057204 (2013).

32. Y. Lao, F. Caravelli, M. Sheikh, J. Sklenar, D. Gardeazabal, J. D. Watts, A. M. Albrecht, A. Scholl, K. Dahmen, C. Nisoli, and P. Schiffer, Classical topological order in the kinetics of artificial spin ice, Nature Physics **14**, 723 (2018).

33. X. Zhang, A. Duzgun, Y. Lao, S. Subzwari, N. S. Bingham, J. Sklenar, H. Saglam, J. Ramberger, J. T. Batley, J. D. Watts, D. Bromley, R. V. Chopdekar, L. O'Brien, C. Leighton, C. Nisoli & P. Schiffer, String Phase in an Artificial Spin Ice, Nature Communications **12**, 6514 (2021).

34. A. P. Ramirez, A. Hayashi, R. J. Cava, R. Siddharthan, and B. S. Shastry, Zero-point entropy in 'spin ice', Nature **399**, 333 (1999).

35. A. D. King, C. Nisoli, E. D. Dahl, G. Poulin-Lamarre, and A. Lopez-Bezanilla, Gauge-free duality in pure square spin ice: Topological currents and monopoles, Science **373**, 576 (2021).

METHODS

Arrays of tetris artificial spin ice with various lateral dimensions and thicknesses were fabricated on silicon (Si) substrates with native oxide using electron beam lithography and lift-off as described in previous work [i,ii,iii]. The bilayer e-beam resist was spin-coated onto the substrate and exposed to the electron beam to write the desired structures. After development, permalloy ($Ni_{80}Fe_{20}$) films with varying thicknesses (2.5 nm – 3.5 nm) were deposited by ultrahigh vacuum electron beam evaporation at a rate of 0.5 Å/s. The base pressure of the system was 10^{-11} – 10^{-10} Torr with a deposition pressure 10^{-10} – 10^{-9} Torr. Subsequently, a 2 nm capping layer of Al was deposited to prevent oxidation of the permalloy. The lattice constants and island sizes were measured using scanning electron microscopy (SEM) and determined to be 602, 606, 806 nm, and 157 x 433, 157 x 433, 178 nm x 483 nm for samples A, B, C, respectively. Further details of the samples can be found in Table SI. 1.1 in the Supplementary Information.

We performed X-ray magnetic circular dichroism-photoemission electron microscopy (XMCD-PEEM) experiments on our tetris ice arrays at the PEEM-3 station at beamline 11.0.1.1 of the Advanced Light Source at Lawrence Berkley National Laboratory. Magnetic imaging was carried out at the Fe L3 edge. We conducted two XMCD-PEEM runs using different X-ray polarization sequences, exposure times, and temperature ranges. The details of the XMCD-PEEM measurements can be found in Table SI. 2.1 in the Supplementary Information.

Methods References

i. I. Gilbert, Y. Lao, I. Carrasquillo, L. O'Brien, J. D. Watts, M. Manno, C. Leighton, A. Scholl, C. Nisoli, and P. Schiffer, Emergent reduced dimensionality by vertex frustration in artificial spin ice, Nature Physics **12**, 162 (2016).

ii. Y. Lao, F. Caravelli, M. Sheikh, J. Sklenar, D. Gardeazabal, J. D. Watts, A. M. Albrecht, A. Scholl, K. Dahmen, C. Nisoli, and P. Schiffer, Classical topological order in the kinetics of artificial spin ice, Nature Physics **14**, 723 (2018).

iii. X. Zhang, A. Duzgun, Y. Lao, S. Subzwari, N. S. Bingham, J. Sklenar, H. Saglam, J. Ramberger, J. T. Batley, J. D. Watts, D. Bromley, R. V. Chopdekar, L. O'Brien, C. Leighton, C. Nisoli, and P. Schiffer, String Phase in an Artificial Spin Ice, Nature Communications **12**, 6514 (2021).